A non-symmetric room-temperature tristriazolotriazine liquid crystal

Monike da Silva Kutz, Luis Augusto Suassuna E Bega, Carolina Francener, Giliandro Farias, Feik Amil de Campos, Harald Bock, Ivan Bechtold, Fernando Molin, Eduard Westphal

A non-symmetric room-temperature tristriazolotriazine liquid crystal

Monike da Silva Kutz [a,b,c], Luis Augusto Suassuna e Bega [a], Carolina Francener [c], Giliandro Farias [d], Feik Amil de Campos [c], Harald Bock [b], Ivan H. Bechtold [e], Fernando Molin [a,*], Eduard Westphal [a,c,*]

[a] Academic Department of Chemistry and Biology, Universidade Tecnológica Federal do Paraná, Curitiba, Brazil
[b] Centre de Recherche Paul Pascal, Université de Bordeaux/Centre National de la Recherche Scientifique, Pessac, France
[c] Department of Chemistry, Universidade Federal de Santa Catarina, Florianópolis, Brazil
[d] Department of Materials Physics and Mechanics, Universidade de São Paulo, São Paulo, Brazil
[e] Department of Physics, Universidade Federal de Santa Catarina, Florianópolis, Brazil

ARTICLE INFO

Keywords:
Heterocycles
Liquid crystals
Tristriazolotriazine
Luminescence
Symmetry

ABSTRACT

Tristriazolotriazine (TTT) has emerged as an easily accessible electron-deficient heterocyclic core for discotic liquid crystals (LCs). Materials that are liquid-crystalline at room temperature, *i.e.*, do not crystallize in ambient conditions, are of particular interest when the LC state is prone to offer advantages in optoelectronic devices, *e.g.*, for anisotropic charge or exciton transport, or anisotropic light emission. However, there has been no report of non-symmetric TTT LCs, *i.e.*, with unequal arms. Here, we report two non-symmetric compounds derived from the TTT core. Their non-symmetry, combined with a high number of peripheral alkyl chains, is found to promote Col_h mesomorphism over a broad temperature range including room temperature. The non-symmetry also induces an increase in the emission quantum yield, compared to symmetric analogs.

1. Introduction

First reported in 1911 by Erhart, then in 1961 by Huisgen, [1] and only since 2008 as the core of discotic liquid crystals, [2] the N-heterocyclic polycyclic compound tris-[1,2,4]-triazolo-[1,3,5]-triazine (tristriazolotriazine or TTT) has been gaining increasing attention for various applications beyond LCs. For example, TTT derivatives have recently been found to show thermally activated delayed fluorescence (TADF) [3,4] and room temperature phosphorescence in solution [5].

In the field of liquid crystals, numerous structural modifications of TTT have been explored, including variations in the type, [6] number, and length of the mesophase-inducing peripheral chains, [1,7,8] and expansion of the rigid core with condensed rings, [9] arylethynyl groups, [10] or benzoate substituents, [11] and even isomerization [12, 13]. These modifications have in some cases led to a substantial lowering of the melting temperature, resulting in mesophases at room temperature, albeit at the expense of the quantum yield of luminescence [11]. Such a decrease in emission yield may be avoided by lowering the molecular symmetry as a means for suppressing crystallization [14-17]. However, to date, there has been no description of non-symmetric TTTs, *i.e.*, those with unequal arms. Therefore, this work aims to fill this gap by reporting two molecules that feature one of the arms of the TTT core being different from the others (Fig. 1).

As triply aryl substituted TTTs are commonly synthesized by condensation of an appropriately substituted aryltetrazole precursor with cyanuric chloride, a straightforward approach to low-symmetry TTTs is the concurrent condensation of two differently substituted aryltetrazoles with cyanuric chloride. The use of two aryltetrazoles bearing different numbers of LC-favoring alkoxy chains is not only appropriate in view of inducing a room temperature mesophase but is also prone to distinguish the different statistical co-trimerization products by their molecular size, facilitating their separation by size-exclusion chromatography.

2. Results and discussion

2.1. Synthesis

The synthesis of non-symmetrically substituted tristriazolotriazines was carried out in two stages: first, the synthesis of tetrazoles with one (**1**) and three (**2**) long alkoxy chains by established procedures (Scheme 1) [11,18], and, second, the reaction of both tetrazoles in equimolar

* Corresponding authors.
E-mail addresses: fmolin@utfpr.edu.br (F. Molin), eduard.w@ufsc.br (E. Westphal).

quantities with cyanuric chloride (**3**) in the presence of K_2CO_3 in refluxing butanone for 22 hours. By this procedure, four different products were obtained: two symmetric compounds (**111** and **333**, previously reported as **3d** and **TTT-345**), and the two desired non-symmetric ones (**311** and **331**). The products were initially purified by column chromatography on silica, and then separated by gel permeation chromatography. The ^{1}H and ^{13}C NMR, HRMS and FT-IR spectra for the new compounds are analytically described in the experimental section, while the spectra of all can be viewed in the SI (Figs. S1-S10).

2.2. *Mesomorphic behavior*

After synthesis and purification, the phase behavior of compounds **311** and **331** was investigated by polarized optical microscopy (POM) and differential scanning calorimetry (DSC) (Table 1). The mesomorphic compound **331** was further studied by X-ray diffraction (XRD), using both wide-angle and small-angle X-ray scattering (WAXS and SAXS, the latter with synchrotron radiation).

As reported previously, the symmetric compound **111**, with three alkoxy peripheral chains, did not exhibit mesomorphism. The material showed only a Cr – Iso phase transition at 86.6 °C during the first DSC heating scan, and then remained liquid upon cooling to room temperature. In subsequent thermal scans, no other phase transitions were observed, and no liquid-crystalline texture was observed by POM [2].

The non-symmetric compound with five alkoxy chains, **311**, appeared waxy at room temperature. Even though birefringence was observed by POM before the first heating, it was absent upon cooling after melting. This was confirmed by DSC, which showed an irreversible transition to the isotropic liquid at 51 °C (Fig. S11), approximately 35 °C lower than the melting of **111**. After the first melting, no crystallization was detected for **311** neither on cooling to -40 °C nor on waiting for several days.

The presence of a second arm containing three long alkoxy chains in compound **331** resulted in stable mesomorphism over a wide temperature range, including room temperature. Upon cooling below the liquid-to-mesophase transition temperature of 180 °C, POM showed growth of large dendritic domains in homeotropic alignment (Fig. 2a), as well as strongly birefringent fanlike domains with linear defects (Fig. 2b), both textures suggesting the formation of a columnar hexagonal (Col_h) mesophase. On gradual cooling, **331** retains the same texture observed at higher temperatures with subtle birefringence changes during the cooling process (Fig. S12 a-e). At room temperature, when the glass coverslip was sheared, the texture was destroyed, demonstrating the fluidity of the phase and absence of crystallization or glass formation (Fig. S12f).

DSC analyses were performed for **331** in order to verify phase transitions previously identified by POM observations, in addition to trying to determine the melting temperature (T_m) of the material. The DSC trace on heating of **331** (Fig. 2c) shows that the material presents two phase transitions, the first one being of high energy (19.7 kJ mol^{-1}) at -13 °C, possibly related to the material's melting. The other transition, of lower energy (7.9 kJ mol^{-1}), is observed at 201 °C, which agrees with the clearing temperature (T_{cl}) observed by POM. The transition pattern persists during cooling and subsequent heating/cooling cycles, with only a small thermal hysteresis between transitions. In contrast, the reported symmetric compound **333**, with nine alkoxy chains, exhibited a Col_h mesophase range between 133 and 177 °C (Table 1). Therefore, the width of the mesomorphic range increases from less than 50 °C for **333** to over 200 °C for **331**.

To confirm the hexagonal symmetry of the columnar mesophase, X-ray diffraction (WAXS and SAXS) was performed at different temperatures. After cooling from the isotropic phase, at 100 °C (Fig. 3b and Table 2), the diffractogram showed a typical Col_h pattern with an intense peak in the small-angle region at 2.70 nm, and three weak peaks at 1.56, 1.36 and 1.03 nm, whose ratios of $1:3^{1/2}:2:7^{1/2}$, allowed a indexation as (10), (11), (20) and (21) reflections of a two-dimensional hexagonal lattice. In the wide-angle regions, two distinct broad peaks were observed at 100 °C: a very broad peak around 0.46 nm, attributed to the disordered liquid-like contacts of the long alkoxy chains, and a second, less broad one, at 0.35 nm, from the disk-to-disk spacing of adjacent molecules within the columns (π-stacking) [19].

From the average values of the diffraction peaks, the lattice parameter (α_h), which corresponds to the distance between nearest columns, was determined to be 3.13 nm at 100 °C, which is smaller than the diameter of the most extended molecular conformation (L = 4.04 nm) [20]. This indicates that the peripheral alkoxy chains are not in their most extended conformation or that they interdigitate between adjacent columns.

By SAXS measurements using synchrotron radiation (Fig. S13 and Table S1), the evolution of the diffractogram upon cooling from the isotropic liquid was analyzed (Fig. S14). As the sample was cooled from 200 °C, α_h increases consistently until reaching a value above 3.15 nm close to 70 °C, and then remains constant at lower temperatures (Fig. 3c). The increase of the column-to-column distance on cooling may be attributed to more extended configurations of the peripheral chains at lower temperatures, leading to an increase in the disk diameter.

The value of α_h for **331** is very similar to that found for the symmetric product **333** (α_h = 3.12 nm) [11], demonstrating that the elimination of two alkoxy chains in one of the arms of the disk does not shrink its diameter, probably because the other side chains spread better. The non-symmetry and lower number of alkoxy chains favors better intracolumnar packing (π-stacking) for **331**, in comparison with **333**, since for the former of periodic packing at 0.35 nm was observed, while no disk-to-disk peak was observed for the latter [11]. Less crowding from fewer peripheral alkoxy chains allows the phenyl rings more space to adopt a slightly more planar conformation, leading to a more regular and potentially tighter disk stacking.

To gain additional insight into how the molecules organize themselves within the columns during the mesophase, the number of molecules that constitute a single disk (Z) was verified for **331** by calculating the resulting density (details in the SI). We initially assumed that a disk

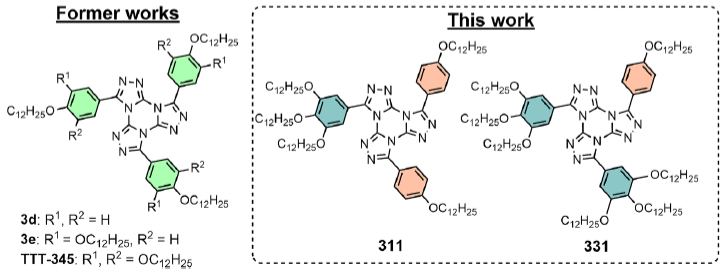

Fig. 1. Structure of the TTT derivatives with C3 symmetry previously reported by our group (**3d**, **3e** and **TTT-345**) [2,11] and the non-symmetric derivatives reported here (**311** and **331**).

is constituted by a single **331** mesogen, as previously described in the literature for the **TTT-345** compound [11]. This assumption yielded a density of 0.969 *g* cm^{-3}, which is a typical density for discotic materials with a large amount of peripheral saturated alkyl moieties [8]. This result confirms that each disc is made up of a single molecule, as any other value of Z would result in an unrealistic density for this type of material.

2.3. Photophysical investigations

The absorption and fluorescence spectra (Fig. 4) for the non-symmetric TTTs (**311** and **331**) were obtained both in chloroform solution (1×10^{-5} mol L^{-1}) and in the solid state (spin-coated films) (Table 3). In solution (Fig. 4a), all compounds absorb strongly (2.6 - 4.4 $\times 10^4$ L mol^{-1} cm^{-1}) in the UV region (294 – 303 nm), indicating $\pi - \pi^*$ transitions. As the number of alkoxy substituents increases from **111** to **333**, a slight bathochromic shift was observed in the absorption spectra, both in solution and in thin film. The emission is predominantly in the UV region, with edges reaching the visible. Although **111** and **333** absorb at similar wavelengths (294-303 nm), they emit at different wavelengths: 362 nm for **111** and 403 nm for **333**. Compounds **311** and **331**, which contain both monoalkoxyphenyl and trialkoxyphenyl arms, emit only from the lower energy band originating from the 3-chain arm, around 403 nm.

For thin films (Fig. 4b), the increase in the number of trialkoxyphenyl groups promotes a slight gradual bathochromic shift in the absorption spectrum (Table 3). In the emission spectrum, the band gradually shifts from 371 (**111**), to 395 (**311**) and to 407 nm (**331**). However, for **333**, the emission band returns to 390 nm. As a result, the Stokes shifts ranged from 68 nm to 106 nm in solution and 85 to 108 nm in the solid state.

In solution, the fluorescence quantum yields (Φ_F) were determined using a known method, [19] with 2-(4-biphenylyl)-5-phenyl-1,3,4-oxadiazole (PBD, Φ_F = 0.83) [20] in chloroform solution as standard. Among the compounds studied, the non-symmetric TTTs displayed higher Φ_F in solution, in the range of 0.35-0.5, while **333** showed a particularly low quantum yield of 0.06. In the solid state, Φ_F was 0.29 and 0.38 for non-symmetric **311** and **331**, and 0.27 for symmetric **333**. Φ_F for **111** was not reported.

2.4. Theoretical investigations

Density functional theory (DFT) calculations within B3LYP-D3/def2-TZVP(-f) were performed to rationalize the emissions. The optimized geometry of each compound is shown in Fig. S15. The alkyl chains were replaced by a methyl group to reduce the computation times. The compounds are non-planar, and the dihedral angles between the phenyl rings and the TTT core are 35° ± 1° in all cases. The frontier molecular orbitals for compounds **111, 311, 331** and **333** are shown in Fig. S16. For all compounds, the occupied orbitals are centered over the phenyl moieties with contributions from the attached methoxy groups, whereas the unoccupied orbitals are mostly centered over the TTT core.

Time-dependent density functional theory (TD-DFT) calculations were performed on the optimized ground state geometries to obtain information about the excited states. The calculated absorption spectra are shown in Fig. S17 and agree with the experimental ones. According to Kasha's rule, we can predict the prompt fluorescence behavior by analyzing the S_1 state, and the oscillator strength (*f*) of S_1 is proportional to the decay rate from this state. $f(S_1)$ for each compound is shown in Table S2, along with the TD-DFT difference density plot for the S_1 state. *f* increases from **111** to **311**, decreases to **331**, and further decreases for **333**. The transitions can be attributed to π-π^* transitions due to the large value of *f*, with charge transfer characteristics from anisole-like moieties to the TTT core as shown in the difference density plot. The variance in the calculated *f* agrees very well with the obtained quantum yield in solution. The increased symmetry for **111** or by attaching more methoxy derivative chains for **331** and **333** results in low-lying states almost degenerating with the S_1 state, which decreases the oscillator strength of S_1 and, consequently, the emission rate from this state. Therefore, the higher emission quantum yield observed for **331** is due to the lower symmetry of the molecule and lower degeneracy of the low-lying state (compare Fig. S17 a and b). The lower quantum yield for **333** is

Table 1
Phase transition temperatures with associated enthalpy values.

Compound	Transitions[a,b] - T/°C [ΔH/kJ mol^{-1}]	
	Heating	Cooling
111 [d]	Cr **86.6** Iso [c]	- [c]
311	Cr* **51** [7.7] Iso [c]	- [c]
331	Cr -13 [19.7] Col_h **201** [7.9] Iso	Iso **199** [8.1] Col_h -19 [18.1] Cr
333 [d]	Cr **133** [23.6] Col_h **177** [9.9] Iso	Iso **176** [10.2] Col_h **118** [25.5] Cr

[a] Cr = crystalline phase; Cr* = waxy solid; Col_h = hexagonal columnar phase; Iso = isotropic liquid.
[b] Transitions determined by DSC (peak temperatures) during the second heating/cooling cycle using a heating/cooling rate of 10 °C min^{-1}.
[c] Transitions determined in the first heating due to no crystallization or new melting in subsequent thermal cycles.
[d] The thermal data presented for compounds **111** (**3d**) and **333** (**TTT-345**) were obtained previously [2,11].

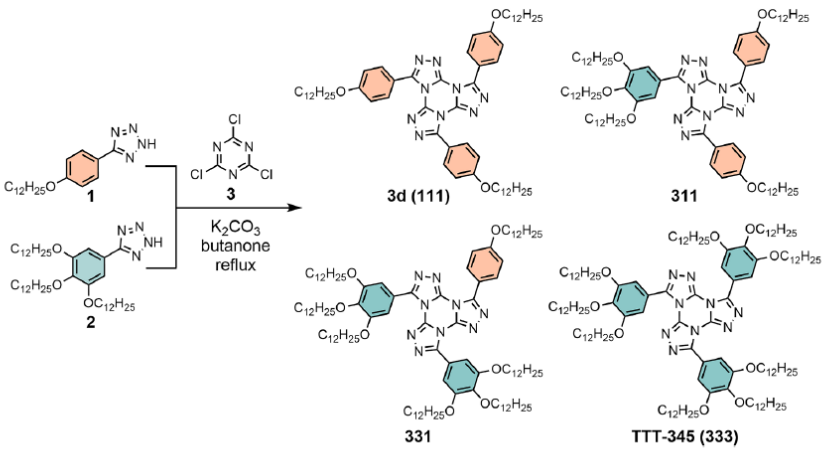

Scheme 1. Synthetic route to symmetric and non-symmetric tris(alkoxyphenyl)tristriazolotriazines.

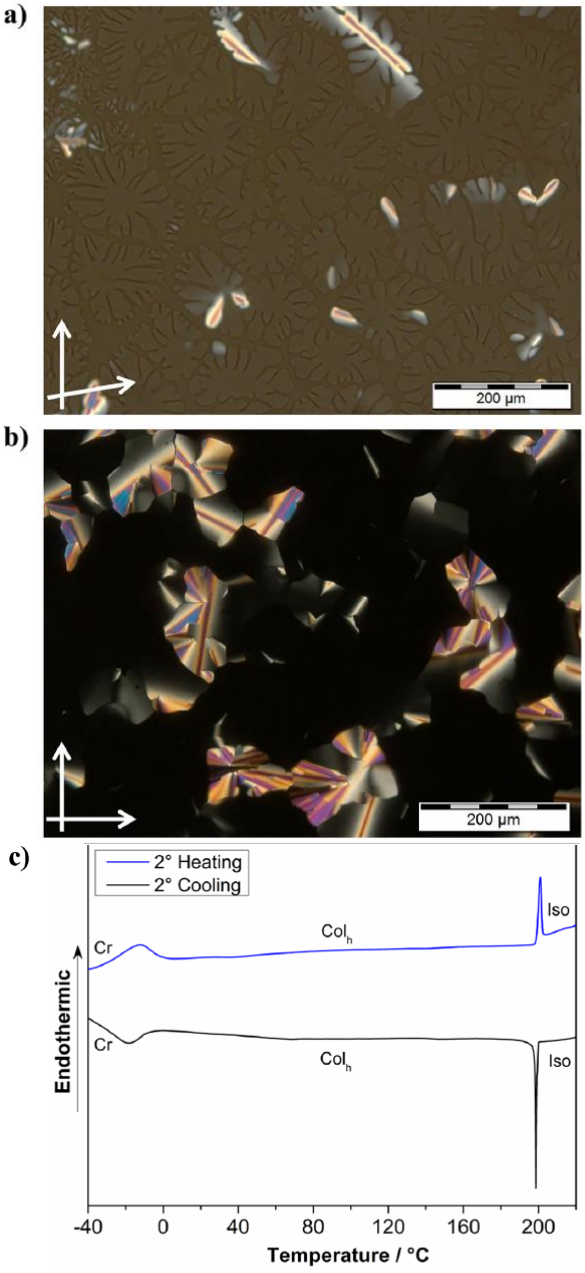

Fig. 2. (a) Textures observed by POM for the liquid-crystalline phase (Col_h) of **331** on cooling from the isotropic liquid at 180 °C (with 10° uncrossed polarizers) showing the homeotropic domain growth, and (b) the characteristic textures at 150 °C (crossed polarizers), along with large regions of homeotropic alignment. (c) DSC thermogram for **331** showing the second heating (blue line) and the second cooling scan (black line), at a rate of 10 °C/min.

attributed to the larger number of alkyl chains, which increases the number of acceptor C-H vibrational modes of higher energy, which is a known path to decrease the emission quantum yield by increasing the non-radiative rate [21]. Despite this, in the solid state, due to the lower mobility of the chains leads to a higher emission for **333**.

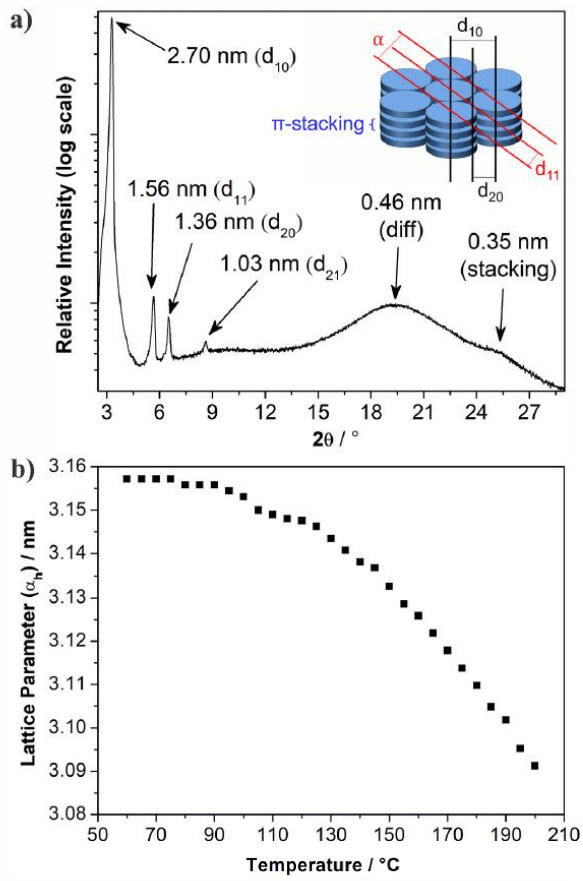

Fig. 3. (a) XRD pattern of the Col_h phase for **331** at 100 °C, after cooling from the isotropic liquid (inset shows the organization of the disks in a Col_h mesophase, with the representation of the main XRD diffractions); (b) Variation of the Col_h lattice parameter (a_h) on cooling from the isotropic liquid, determined by SAXS using synchrotron radiation.

Table 2
XRD data: indexation and calculated lattice parameter (a_h) for **331**.

Phase (T/°C)	d_{obs}/nm (*hk*)	Lattice Parameter a_h/nm [a]
Col_h	2.70 (10)	3.13
(100)	1.56 (11)	
	1.36 (20)	
	1.03 (21)	
	0.46 (*diffuse*)	
	0.35 (*π-stacking*)	

[a] Columnar hexagonal lattice parameter determined by XRD.

3. Conclusions

Two non-symmetric tristriazolotriazine derivatives were synthesized by reacting two differently substituted phenyltetrazoles with cyanuric chloride and subsequently separated by size-exclusion chromatography. Compound **331**, with a periphery of seven alkoxy chains, exhibits a stable Col_h mesophase around and above room temperature, covering a range of more than 200 °C.

The non-symmetric compounds absorb in the range between 290-300 nm and emit in the 400 nm region. In solution, the position of the

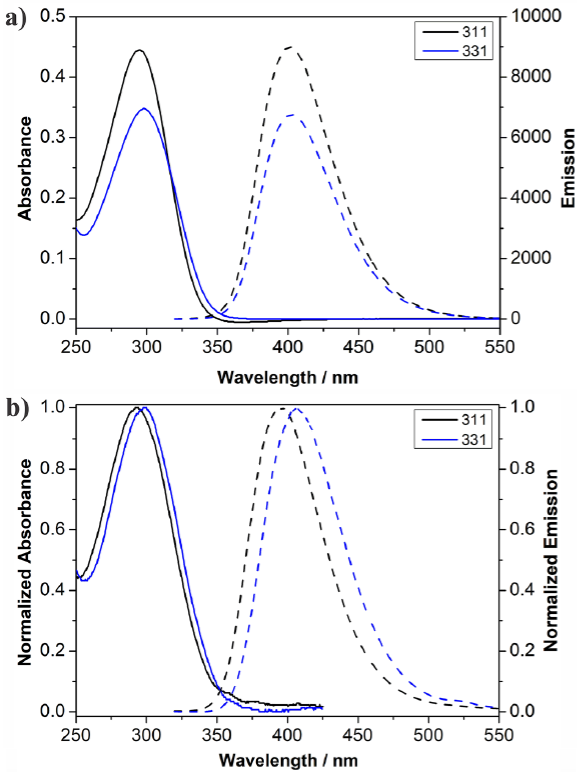

Fig. 4. Normalized absorption (continuous line) and emission (dashed) spectra of **311** (black) and **331** (blue) in a 1×10^{-5} mol L^{-1} chloroform solution (a) and spin-coated films (b).

emission depends primarily on the presence or absence of a trialkoxyphenyl moiety, while in the solid state, a greater number of such moieties leads to a greater red-shift, except for the symmetric compound containing exclusively trialkoxyphenyl arms (**333**), which exhibits a blue shift. The non-symmetric compounds are more luminescent than their symmetric analogs, with quantum yields of 0.35 and 0.50 in chloroform solution, and of 0.29 and 0.38 in spin-coated films. Theoretical calculations show that the distinct behavior of the non-symmetric compounds is primarily due to the degeneracy of the lower energy states, rather than to a significant difference in the torsional angles between the TTT core and the phenyl rings.

This highlights the benefits of molecular non-symmetry in both inducing and stabilizing mesomorphic properties in columnar liquid crystals, as well as enhancing their emission.

4. Experimental

4.1. Materials and characterizations

Reagents and solvents were acquired in analytical grade from commercial sources (Aldrich, Merck, Acros and Vetec) and used without previous purification. Reactions were monitored by Thin Layer Chromatography (TLC) on aluminum plates coated with a thin layer of silica gel 60, with the indicator UV_{254} – Marcherey – Nagel. Purifications were carried out by recrystallization and by column chromatography on silica–gel 60–200 mesh 60 Å using commercial grade solvents, and by Gel Permeation Chromatography (GPC) technique, using JAI FC-3480 Recycling Preparative HPLC in a JAIGEL-2.5HR-40 column, with HPLC-isocratic grade chloroform stabilized with ethanol as eluent.

Infrared (IR) spectra were obtained in a Bruker spectrometer, model Alpha, using KBr pellets. ^{1}H and ^{13}C Nuclear Magnetic Resonance (NMR) spectra were obtained on a JEOL ECS-400 spectrometer operating at 400 MHz and 100.6 MHz, respectively. Chemical shifts (δ) are given in parts per million (ppm) and are relative to tetramethylsilane (TMS) as an internal standard. NMR spectra were obtained using deuterated chloroform ($CDCl_3$) as the solvent. High resolution mass spectra were recorded on a Bruker micrOTOF-Q II mass spectrometer using Atmospheric Pressure Photoionization (APPI) ionization method and operating in positive ion mode.

4.2. Thermal analysis

A polarized optical microscope Olympus BX53 coupled to a Mettler Toledo FP-82 hot stage and an Olympus DP73 digital camera was used to investigate melting point, phase transitions, and mesomorphic textures of all compounds. For the target compounds, thermal transitions and associated enthalpies values were determined by DSC measurements, carried out using a DSC Q2000 calorimeter (TA Instruments) equipped with a RCS90 cooling system, with a heating/cooling rate of 10 °C min^{-1} and a nitrogen flow of 50 mL min^{-1}.

4.3. X-ray diffraction

X-ray diffraction (XRD) measurements were performed with an X'Pert PRO (PANalytical) diffractometer using Cu Kα beam (λ = 1.5418 Å), an applied power of 1.2 kVA and using the X'Celerator detector to collect the diffracted radiation. Films were prepared by depositing an

Table 3
Photophysical properties in chloroform and in spin-coated film.

Compound	Solution				Film[e]			
	Absorption[a] λ_{max}/nm (ε/10^4)[b]	Emission λ_{max}/nm	Stokes Shift[c] /nm	Φ_F[d]	Absorption λ_{max}/nm	Emission λ_{max}/nm	Stokes Shift[c] /nm	Φ_F[f]
111[g]	294	362	68	0.34	286	371	85	-[h]
311	295 (4.4)	401	106	0.52	293	395	102	0.29 ± 0.05
331	298 (3.5)	403	105	0.35	299	407	108	0.38 ± 0.06
333[g]	303 (2.6)	403	100	0.06	304	390	86	0.27 ± 0.06

[a] Determined in $CHCl_3$ solution (1×10^{-5} mol L^{-1}).
[b] Unit = L mol^{-1} cm^{-1}.
[c] Difference between emission maximum and longest wavelength maximum of absorption spectra.
[d] Quantum yield of fluorescence in $CHCl_3$ solution relative to PBD in $CHCl_3$ ($\Phi_F = 0.83$) as standard.
[e] Prepared by the spin-coating on a quartz substrate.
[f] Absolute quantum yield of fluorescence.
[g] The photophysical data presented for compounds **111** (**3d**) and **333** (**TTT-345**) were taken from [2,11].
[h] Not determined.

amount of powder on a glass plate, where the temperature was controlled with a TCU2000 – Temperature Control Unit (Anton Paar). The scan was carried out in continuous mode from 2° to 30° (2θ angle) with the sample in the mesophase, which was obtained by cooling from the isotropic liquid.

Small-angle X-ray scattering (SAXS) measurements were performed on the SAXS1 beamline at the Brazilian Synchrotron Light Laboratory (LNLS), CNPEM/MCTIC, using a wavelength 1.544 Å. The samples were placed inside a 1.5 mm quartz capillary (Hampton Research) and inserted into the Linkam Scientific DSC6000 furnace coupled to a LNP95 cooling system. The scattered beam was detected on a Pilatus 300k detector, with a sample-to-detector distance of 806 mm, calibrated with silver behenate powder. The **331** sample was heated to the isotropic liquid and cooled at a rate of 5 °C min^{-1}, with a continuous acquisition time of 20 s followed by 40 s pause.

4.4. Photophysical investigations

The absorption and photoluminescence spectra both in solution and in thin solid film were recorded in the UV-Vis region by using a Shimadzu 2600i spectrophotometer and a Hitachi F-7000 fluorimeter, respectively.

All compounds studied were dissolved in $CHCl_3$ at 1×10^{-5} mol L^{-1}, except in quantum yield measurements, which had their concentrations adjusted as needed. The relative fluorescence quantum yields (Φ_F) were calculated according to a known procedure, [22] using 2-(4-biphenylyl)-5-phenyl-1,3,4-oxadiazole (PBD) in $CHCl_3$ ($\Phi_F = 0.83$) as standard, due to its photophysical similarities [23].

For the measurements on thin solid films, quartz substrates were cleaned by subsequent ultrasonication in a detergent solution, distilled water, and ethanol, for 10 minutes each. Then, the substrates were dried and treated with ultraviolet-ozone surface cleaner, for 4 minutes. The compounds were dissolved in chloroform (10 mg mL^{-1}) and 100 μL were spin-coated onto the quartz substrates at 2000 rpm for 30 s. The absolute quantum yields for the spin-coated films were measured on a Hamamatsu Photonics c9920-02G spectrophotometer with a 150W xenon light source.

4.5. DFT methodology

The geometries of compounds **111, 311, 331** and **333** were optimized at the density functional theory (DFT) level using the B3LYP [24, 25] and def2-TZVP(-f) basis set for all atoms [26-28]. Dispersion effects (if present) were included using Grimme's D3 correction with the Becke-Johnson (BJ) damping [29,30]. The evaluation of the four-center integrals was accelerated with the RIJCOSX algorithm, using the resolution-of-the-identity approximation for the Coulomb part (RIJ) and the chain of spheres approach for the Fock exchange (COSX) [31,32]. RIJ requires the specification of an auxiliary basis set for the Coulomb part (Def2/J) and a numerical integration grid for the exchange part (DefGrid-2) [33]. Analytical harmonic vibrational frequency calculations were conducted to verify if the ground state is at the minimum on the potential energy surface. Time-dependent density functional theory under the Tamm-Dancoff approximation (TD-DFT/TDA) [34] was employed to obtain the first 30 excitations using the same calculation protocol to simulate the absorption spectra. The linear response conductor-like polarizable continuum model (LR-CPCM) [35] method included solvent effects in the excited state energies, adopting chloroform as the solvent. All these calculations were performed using Orca 5.0.4, [36] and the geometric representations of the complexes were obtained using the Chemcraft software [37].

4.6. Synthesis and characterization

Synthesis of target compounds: To a 125 mL round-bottomed flask were added 5-[4-(dodecyloxy)phenyl]-1H-tetrazole (**2**) (0.42 g, 330.24 g mol^{-1}, 1.26 mmol), 5-[3,4,5-*tris*(dodecyloxy)phenyl]-1H-tetrazole (**6**) (0.88 g, 698.61 g mol^{-1}, 1.26 mmol), dry K_2CO_3 (0.70 g, 138.20 g mol^{-1}, 5.0 mmol), cyanuric chloride (0.153 g, 182.92 g mol^{-1}, 0.8 mmol) and anhydrous butanone (60 mL). The heterogeneous mixture was refluxed for 22 hours and then cooled to room temperature. The insoluble part was removed by vacuum filtration, the solid was washed with DCM and the combined organic solvents was removed under reduced pressure. The crude product was initially purified by column chromatography on silica in DCM and then by GPC in HPLC-isocratic grade chloroform.

Compound 111: Yield: 58.1 mg (982.41 g mol^{-1}, 0.06 mmol, 7%). Characterization data consistent with those found in the literature [2].

Compound 311: Yield: 164.3 mg (1351.06 g mol^{-1}, 0.12 mmol, 15%). **m.p.**: see Table 1. **IR** (KBr disk) ν_{max} cm^{-1}: 2956, 2923, 2854, 1611, 1595, 1487, 1468, 1431, 1338, 1254, 1181, 1116, 834. **^{1}H NMR** (400 MHz, $CDCl_3$) δ ppm: 0.79 – 0.83 (m, 15H, -CH_3), 1.18 – 1.31 (m, 80H, -CH_2-), 1.35 – 1.45 (m, 10H, -$CH_2CH_2CH_2O$-), 1.66 – 1.79 (m, 10H, -CH_2CH_2O-), 3.97 – 4.00 (m, 10H, -CH_2O-), 6.98 (d, $J = 8.4$ Hz, 2H, Ar-H), 6.99 (d, $J = 8.4$ Hz, 2H, Ar-H), 7.43 (s, 2H, Ar-H), 8.02 (d, $J = 8.4$ Hz, 4H, Ar-H). **^{13}C NMR** (100.6 MHz, $CDCl_3$) δ ppm: 14.22, 22.79, 26.13, 26.21, 29.24, 29.39, 29.48, 29.55, 29.65, 29.72, 29.77, 29.81, 29.87, 30.46, 32.03, 68.35, 69.38, 73.73, 108.69, 114.55, 115.85, 118.41, 131.99, 140.51, 140.68, 141.19, 150.97, 151.11, 151.14, 153.03, 162.16. **Q-TOF/MS** APPI: m/z for $C_{84}H_{136}N_9O_5^+$ $[M+H]^+$: Calculated: 1351.0659; 1351.0619.

Compound 331: Yield: 254.5 mg (1719.71 g mol^{-1}, 0.15 mmol, 18%). **m.p.**: see Table 1. **IR** (KBr disk) ν_{max} cm^{-1}: 2956, 2923, 2854, 1613, 1597, 1578, 1489, 1469, 1432, 1340, 1254, 1116, 834. **^{1}H NMR** (400 MHz, $CDCl_3$) δ ppm: 0.79 – 0.83 (m, 21H, -CH_3), 1.18 – 1.30 (m, 112H, -CH_2-), 1,37 – 1,44 (m, 14H, -$CH_2CH_2CH_2O$-), 1.67 – 1.80 (m, 14H, -CH_2CH_2O), 3.97 – 4.02 (m, 14H, -CH_2O-), 7,00 (d, $J = 8.4$ Hz, 2H, Ar-H), 7,38 (s, 2H, Ar-H), 7,41 (s, 2H, Ar-H), 8,02 (d, $J = 8.4$ Hz, 2H, Ar-H). **^{13}C NMR** (100.6 MHz, $CDCl_3$) δ ppm: 14.21, 22.78, 26.12, 26.19, 26.22, 29.23, 29.42, 29.46, 29.50, 29.54, 29.67, 29.71, 29.76, 29.81, 29.86, 68.36, 69.39, 69.42, 73.74, 108.76, 108.83, 114.57, 115.78, 118.31, 118.36, 132.03, 140.60, 140.77, 141.30, 141.38, 151.13, 151.19, 151.32, 153.06, 153.12, 162.18. **Q-TOF/MS** APPI: m/z for $C_{108}H_{184}N_9O_7^+$ $[M+H]^+$: Calculated: 1719.4313; Found: 1719.4261.

Compound 333: Yield: 168.7 mg (2088.35 g mol^{-1}, 0.08 mmol, 10%). Characterization data consistent with those found in the literature [11].

CRediT authorship contribution statement

Monike da Silva Kutz: Writing – original draft, Visualization, Investigation, Formal analysis. **Luis Augusto Suassuna e Bega:** Investigation, Formal analysis. **Carolina Francener:** Investigation, Formal analysis. **Giliandro Farias:** Writing – review & editing, Investigation, Formal analysis. **Feik Amil de Campos:** Investigation, Formal analysis. **Harald Bock:** Writing – review & editing, Supervision. **Ivan H. Bechtold:** . **Fernando Molin:** Writing – review & editing, Supervision, Project administration, Investigation. **Eduard Westphal:** Writing – original draft, Supervision, Project administration, Investigation, Funding acquisition, Formal analysis, Data curation.

Declaration of competing interest

The authors declare that they have no known competing financial interests or personal relationships that could have appeared to influence the work reported in this paper.

Data availability

Data will be made available on request.

Acknowledgments

The authors thank to CNPq/Proc. 311239/2022-6 and 409209/2023-6, CAPES/COFECUB/project 937-20 and Ph-C 962/20, INCT/INEO, and INCT-Catálise for financial support. Laboratório de Difração de Raios X (LDRX/UFSC) for the XRD experiments, Brazilian Synchrotron Light Laboratory (LNLS) due to the access to the SAXS1 beamline (Proposal 20170154) and Laboratório de Biologia Molecular Estrutural (LABIME) for the HRMS analysis.

Supplementary materials

Supplementary material associated with this article can be found, in the online version, at doi:10.1016/j.molstruc.2024.139996.

References

[1] H. Detert, Tristriazolotriazines: luminescent discotic liquid crystals, Eur. J. Org. Chem. (33) (2018) 4501–4507, https://doi.org/10.1002/ejoc.201800671, 2018.
[2] R. Cristiano, H. Gallardo, A.J. Bortoluzzi, I.H. Bechtold, C.E.M. Campos, R. L. Longo, Tristriazolotriazines: a core for luminescent discotic liquid crystals, Chem. Commun. 41 (2008) 5134–5136, https://doi.org/10.1039/b810680k.
[3] S. Wang, X. Wang, K.H. Lee, S. Liu, J.Y. Lee, W. Zhu, Y. Wang, Blue thermally activated delayed fluorescence based on tristriazolotriazine core: synthesis, property and the application for solution-processed OLEDs, Dyes Pigm. 182 (2020) 108589, https://doi.org/10.1016/j.dyepig.2020.108589.
[4] F. Hundemer, E. Crovini, Y. Wada, H. Kaji, S. Bräse, E. Zysman-Colman, Tris (triazolo)triazine-based emitters for solution-processed blue thermally activated delayed fluorescence organic light-emitting diodes, Mater. Adv. 1 (8) (2020) 2862–2871, https://doi.org/10.1039/D0MA00659A.
[5] H. Marchi Luciano, G. Farias, C.M. Salla, L.G. Franca, S. Kuila, A.P. Monkman, F. Durola, I.H. Bechtold, H. Bock, H. Gallardo, Room temperature phosphorescence in solution from thiophene-bridged triply donor-substituted tristriazolotriazines, Chem. Eur. J. 29 (23) (2023) e202203800, https://doi.org/10.1002/chem.202203800.
[6] R. Cristiano, J. Ecther, I.H. Bechtold, C.N. Tironi, A.A. Vieira, F. Molin, H. Gallardo, Luminescent columnar liquid crystals based on tristriazolotriazine, Langmuir 28 (31) (2012) 11590–11598, https://doi.org/10.1021/la3020139.
[7] T. Rieth, S. Glang, D. Borchmann, H. Detert, 3,5-Dialkoxy substituted triphenyl-tristriazolotriazines: fluorescent discotic liquid crystals, Mol. Cryst. Liq. Cryst. 610 (1) (2015) 89–99, https://doi.org/10.1080/15421406.2015.1025210.
[8] T. Rieth, N. Tober, D. Limbach, T. Haspel, M. Sperner, N. Schupp, P. Wicker, S. Glang, M. Lehmann, H. Detert, Impact of substitution pattern and chain length on the thermotropic properties of alkoxy-substituted triphenyl-tristriazolotriazines, Molecules 25 (23) (2020) 5761, https://doi.org/10.3390/molecules25235761.
[9] T. Rieth, T. Marszalek, W. Pisula, H. Detert, Thermotropic properties and molecular packing of discotic tristriazolotriazines with rigid substituents, Chem. Eur. J. 20 (17) (2014) 5000–5006, https://doi.org/10.1002/chem.201400034.
[10] S. Glang, T. Rieth, D. Borchmann, I. Fortunati, R. Signorini, H. Detert, Arylethynyl-substituted tristriazolotriazines: synthesis, optical properties, and thermotropic behavior, Eur. J. Org. Chem. (15) (2014) 3116–3126, https://doi.org/10.1002/ejoc.201400088, 2014.
[11] E. Westphal, A.C. Windisch, D.Z. Mezalira, H. Gallardo, Reaching room-temperature mesomorphism through expansion of the tristriazolotriazine core with alkoxybenzoate units, Eur. J. Org. Chem. 2022 (29) (2022) e202200378, https://doi.org/10.1002/ejoc.202200378.
[12] M. Jochem, D. Limbach, S. Glang, T. Haspel, H. Detert, Experimental and theoretical investigation on the thermal isomerization reaction of tristriazolotriazines, J. Phys. Org. Chem. 35 (7) (2022) e4346, https://doi.org/10.1002/poc.4346.
[13] T. Rieth, N. Röder, M. Lehmann, H. Detert, Isomerisation of liquid-crystalline tristriazolotriazines, Chem. Eur. J. 24 (1) (2018) 93–96, https://doi.org/10.1002/chem.201705095.
[14] J.A. Rego, S. Kumar, H. Ringsdorf, Synthesis and characterization of fluorescent, low-symmetry triphenylene discotic liquid crystals: tailoring of mesomorphic and optical properties, Chem. Mater. 8 (7) (1996) 1402–1409, https://doi.org/10.1021/cm950582x.
[15] H. Bock, M. Rajaoarivelo, S. Clavaguera, É. Grelet, An efficient route to stable room-temperature liquid-crystalline triphenylenes, Eur. J. Org. Chem. (13) (2006) 2889–2893, https://doi.org/10.1002/ejoc.200600116, 2006.
[16] M. Chen, T.-R. Zhang, W.-H. Yu, Q.-G. Li, S.-K. Xiang, P. Cao, K.-Q. Zhao, C. Feng, B.-Q. Wang, Hydrogen-bonding stabilized columnar mesophases in hexasubstituted triphenylene 2,3-dicarboxamides, J. Mol. Liq. 366 (2022) 120122, https://doi.org/10.1016/j.molliq.2022.120122.
[17] P.J. Stackhouse, M. Hird, Influence of branched chains on the mesomorphic properties of symmetrical and unsymmetrical triphenylene discotic liquid crystals, Liq. Cryst. 35 (5) (2008) 597–607, https://doi.org/10.1080/02678290802040026.
[18] A.B.S. Santos, A.M. Manfredi, C.A.M. Salla, G. Farias, E. Girotto, J. Ecther, E. Westphal, S.F. Curcio, T. Cazati, I. Malvestiti, E.H.L. Falcão, I.H. Bechtold, H. Gallardo, Highly luminescent liquid crystals by connecting 1,3,4-oxadiazole with thiazolo[5,4-d]thiazole units, J. Mol. Liq. 321 (2021) 114887, https://doi.org/10.1016/j.molliq.2020.114887.
[19] S. Laschat, A. Baro, N. Steinke, F. Giesselmann, C. Hägele, G. Scalia, R. Judele, E. Kapatsina, S. Sauer, A. Schreivogel, M. Tosoni, Discotic liquid crystals: from tailor-made synthesis to plastic electronics, Angew. Chem., Int. Ed 46 (26) (2007) 4832–4887, https://doi.org/10.1002/anie.200604203.
[20] Molecular length was estimated with the ChemBio3D Ultra software (version 14.0) and assuming the molecule to be in the most stretched conformation.
[21] N.J. Turro, V. Ramamurthy, J.C. Scaiano, Modern Molecular Photochemistry of Organic Molecules, University Science Books, Sausalito, 2010.
[22] S. Fery-Forgues, D. Lavabre, Are fluorescence quantum yields so tricky to measure? a demonstration using familiar stationery products, J. Chem. Educ. 76 (9) (1999) 1260–1264, https://doi.org/10.1021/ed076p1260.
[23] D.F. Eaton, Reference materials for fluorescence measurement, Pure Appl. Chem. 60 (7) (1988) 1107–1114, https://doi.org/10.1351/pac198860071107.
[24] A.D. Becke, Density-functional exchange-energy approximation with correct asymptotic behavior, Phys. Rev. A 38 (6) (1988) 3098–3100, https://doi.org/10.1103/PhysRevA.38.3098.
[25] C. Lee, W. Yang, R.G. Parr, Development of the Colle-Salvetti correlation-energy formula into a functional of the electron density, Phys. Rev. B 37 (2) (1988) 785–789, https://doi.org/10.1103/PhysRevB.37.785.
[26] A. Schäfer, H. Horn, R. Ahlrichs, Fully optimized contracted Gaussian basis sets for atoms Li to Kr, J. Chem. Phys. 97 (4) (1992) 2571–2577, https://doi.org/10.1063/1.463096.
[27] A. Schäfer, C. Huber, R. Ahlrichs, Fully optimized contracted Gaussian basis sets of triple zeta valence quality for atoms Li to Kr, J. Chem. Phys. 100 (8) (1994) 5829–5835, https://doi.org/10.1063/1.467146.
[28] F. Weigend, R. Ahlrichs, Balanced basis sets of split valence, triple zeta valence and quadruple zeta valence quality for H to Rn: design and assessment of accuracy, Phys. Chem. Chem. Phys. 7 (18) (2005) 3297–3305, https://doi.org/10.1039/B508541A.
[29] S. Grimme, J. Antony, S. Ehrlich, H. Krieg, A consistent and accurate ab initio parametrization of density functional dispersion correction (DFT-D) for the 94 elements H-Pu, J. Chem. Phys. 132 (15) (2010) 154104, https://doi.org/10.1063/1.3382344.
[30] S. Grimme, S. Ehrlich, L. Goerigk, Effect of the damping function in dispersion corrected density functional theory, J. Comput. Chem. 32 (7) (2011) 1456–1465, https://doi.org/10.1002/jcc.21759.
[31] R. Izsák, F. Neese, An overlap fitted chain of spheres exchange method, J. Chem. Phys. 135 (14) (2011) 144105, https://doi.org/10.1063/1.3646921.
[32] R. Izsák, F. Neese, W. Klopper, Robust fitting techniques in the chain of spheres approximation to the Fock exchange: the role of the complementary space, J. Chem. Phys. 139 (9) (2013) 094111, https://doi.org/10.1063/1.4819264.
[33] B. Helmich-Paris, B. de Souza, F. Neese, R. Izsák, An improved chain of spheres for exchange algorithm, J. Chem. Phys. 155 (10) (2021) 104109, https://doi.org/10.1063/5.0058766.
[34] T. Petrenko, S. Kossmann, F. Neese, Efficient time-dependent density functional theory approximations for hybrid density functionals: analytical gradients and parallelization, J. Chem. Phys. 134 (5) (2011) 054116, https://doi.org/10.1063/1.3533441.
[35] R. Cammi, B. Mennucci, J. Tomasi, Fast evaluation of geometries and properties of excited molecules in solution: a Tamm-Dancoff model with application to 4-dimethylaminobenzonitrile, J. Phys. Chem. A 104 (23) (2000) 5631–5637, https://doi.org/10.1021/jp000156l.
[36] F. Neese, Software update: the ORCA program system, version 4.0, WIREs Comput. Mol. Sci. 8 (1) (2018) e1327, https://doi.org/10.1002/wcms.1327.
[37] Chemcraft - graphical software for visualization of quantum chemistry computations. https://www.chemcraftprog.com.